

Metal Chlorides Grafted on SAPO-5 (MCl_x/SAPO-5) as Reusable and Superior Catalysts for Acylation of 2-Methylfuran Under Non-Microwave Instant Heating Condition

Authors:

Ismail Alhassan Auwal, Ka-Lun Wong, Tau Chuan Ling, Boon Seng Ooi, Eng-Poh Ng

Date Submitted: 2020-07-17

Keywords: non-microwave instant heating, acylation, thermochemical activation, grafting, metal chloride, silicoaluminophosphate number 5 (SAPO-5)

Abstract:

Highly active metal chlorides grafted on silicoaluminophosphate number 5, MCl_x/SAPO-5 (M = Cu, Co, Sn, Fe and Zn) catalysts via simple grafting of respective metal chlorides (MCl_x) onto SAPO-5 are reported. The study shows that thermochemical treatment after grafting is essential to ensure the formation of chemical bondings between MCl_x and SAPO-5. In addition, the microscopy, XRD and nitrogen adsorption analyses reveal the homogeneous distribution of MCl_x species on the SAPO-5 surface. Furthermore, the elemental microanalysis confirms the formation of Si-O-M covalent bonds in ZnCl₂/SAPO-5, SnCl₄/SAPO-5 and FeCl₃/SAPO-5 whereas only dative bondings are formed in CoCl₂/SAPO-5 and CuCl₂/SAPO-5. The acidity of MCl_x/SAPO-5 is also affected by the type of metal chloride grafted. Thus, their catalytic behavior is evaluated in the acid-catalyzed acylation of 2-methylfuran under novel non-microwave instant heating conditions (90-110 °C, 0-20 min). ZnCl₂/SAPO-5, which has the largest amount of acidity (mainly Lewis acid sites), exhibits the best catalytic performance (94.5% conversion, 100% selective to 2-acetyl-5-methylfuran) among the MCl_x/SAPO-5 solids. Furthermore, the MCl_x/SAPO-5 solids, particularly SnCl₄/SAPO-5, FeCl₃/SAPO-5 and ZnCl₂/SAPO-5, also show more superior catalytic performance than common homogeneous acid catalysts (H₂SO₄, HNO₃, CH₃COOH, FeCl₃, ZnCl₂) with higher reactant conversion and catalyst reusability, thus offering a promising alternative for the replacement of hazardous homogeneous catalysts in Friedel-Crafts reactions.

Record Type: Published Article

Submitted To: LAPSE (Living Archive for Process Systems Engineering)

Citation (overall record, always the latest version):

LAPSE:2020.0872

Citation (this specific file, latest version):

LAPSE:2020.0872-1

Citation (this specific file, this version):


LAPSE:2020.0872-1v1

DOI of Published Version: <https://doi.org/10.3390/pr8050603>

License: Creative Commons Attribution 4.0 International (CC BY 4.0)

Article

Metal Chlorides Grafted on SAPO-5 (MCl_x /SAPO-5) as Reusable and Superior Catalysts for Acylation of 2-Methylfuran Under Non-Microwave Instant Heating Condition

Ismail Alhassan Auwal ^{1,2}, Ka-Lun Wong ^{3,4}, Tau Chuan Ling ⁵, Boon Seng Ooi ⁶ and Eng-Poh Ng ^{1,*} 

¹ School of Chemical Sciences, Universiti Sains Malaysia, USM, Penang 11800, Malaysia; sahiburrahmah@gmail.com

² Department of Chemistry, Sule Lamido University, PMB 048, Kafin Hausa 741103, Nigeria

³ School of Energy and Chemical Engineering, Xiamen University Malaysia, Sepang 43900, Malaysia; kalun.wong@xmu.edu.my

⁴ College of Chemistry and Chemical Engineering, Xiamen University, Xiamen 361005, China

⁵ Institute of Biological Sciences, Faculty of Science, University of Malaya, Kuala Lumpur 50603, Malaysia; tcling@um.edu.my

⁶ School of Chemical Engineering, Engineering Campus, Universiti Sains Malaysia, Nibong Tebal, Penang 14300, Malaysia; chobs@usm.my

* Correspondence: epng@usm.my

Received: 27 April 2020; Accepted: 15 May 2020; Published: 19 May 2020



Abstract: Highly active metal chlorides grafted on silicoaluminophosphate number 5, MCl_x /SAPO-5 ($M = Cu, Co, Sn, Fe$ and Zn) catalysts via simple grafting of respective metal chlorides (MCl_x) onto SAPO-5 are reported. The study shows that thermochemical treatment after grafting is essential to ensure the formation of chemical bondings between MCl_x and SAPO-5. In addition, the microscopy, XRD and nitrogen adsorption analyses reveal the homogeneous distribution of MCl_x species on the SAPO-5 surface. Furthermore, the elemental microanalysis confirms the formation of Si–O–M covalent bonds in $ZnCl_x$ /SAPO-5, $SnCl_x$ /SAPO-5 and $FeCl_x$ /SAPO-5 whereas only dative bondings are formed in $CoCl_x$ /SAPO-5 and $CuCl_x$ /SAPO-5. The acidity of MCl_x /SAPO-5 is also affected by the type of metal chloride grafted. Thus, their catalytic behavior is evaluated in the acid-catalyzed acylation of 2-methylfuran under novel non-microwave instant heating conditions (90–110 °C, 0–20 min). $ZnCl_x$ /SAPO-5, which has the largest amount of acidity (mainly Lewis acid sites), exhibits the best catalytic performance (94.5% conversion, 100% selective to 2-acetyl-5-methylfuran) among the MCl_x /SAPO-5 solids. Furthermore, the MCl_x /SAPO-5 solids, particularly $SnCl_x$ /SAPO-5, $FeCl_x$ /SAPO-5 and $ZnCl_x$ /SAPO-5, also show more superior catalytic performance than common homogeneous acid catalysts (H_2SO_4 , HNO_3 , CH_3COOH , $FeCl_3$, $ZnCl_2$) with higher reactant conversion and catalyst reusability, thus offering a promising alternative for the replacement of hazardous homogeneous catalysts in Friedel–Crafts reactions.

Keywords: silicoaluminophosphate number 5 (SAPO-5); metal chloride; grafting; thermochemical activation; acylation; non-microwave instant heating

1. Introduction

Furan and its acylated derivatives are important aromatic compounds that can be found in plants and microorganisms [1,2]. These heterocyclic compounds have widely been used in drug, food, fragrance, petrochemical and fine chemical industries due to their non-polar characteristics,

albeit has the ability to form hydrogen bondings with other polar organic compounds through their ether oxygen atom [3–5]. Typically, acyl furans can be synthesized in laboratory via the Friedel–Crafts acylation of furan with acyl chloride or acetic anhydride using homogeneous Lewis acid (e.g., AlCl_3 , BF_3 , SnCl_4 , ZnCl_2) or Brønsted acid (e.g., H_2SO_4 , HCl , HNO_3) catalysts [6–9]. Nevertheless, the use of homogeneous catalysts suffers from several major drawbacks, including safety issues (high toxicity and corrosive), environmental pollution (large waste production and energy consumption), reaction products separation and catalyst recovery/reusability [10–12].

Zeolites and zeolite-like (AlPO-*n*, SAPO-*n*) solids are crystalline microporous materials composed of tetrahedral networks of TO_4 (T = Si, Al and/or P) [13]. These materials are very promising microporous solids from an environmental point of view, as catalysts, ion exchangers, molecular sieves and catalyst supports owing to their non-toxicity and high reusability [14–17]. Particularly, silicoaluminophosphate number 5 (SAPO-5) solid, which possesses a 12-membered ring and a one-dimensional pore channel system ($0.73 \times 0.73 \text{ nm}^2$), exhibits several benefits over its aluminosilicate zeolite counterpart, such as low synthesis cost (readily use as acid catalyst after calcination and no proton/ammonium ion exchange is needed), high hydrothermal stability [18] and high selectivity to desired products [19]. SAPO-5 has been extensively studied as catalysts and catalyst supports in many organic/inorganic transformation reactions, such as methanol-to-olefin (MTO) conversion [20], methylation of naphthalene [21] and epoxidation of styrene [22]. Nevertheless, a major drawback of SAPO-5 that has been encountered thus far is its mild Brønsted and very weak Lewis acidities, which hardly catalyze some chemical reactions that require strong acidity (e.g., acylation of furan, oligomerization) [23]. Thus, in a quest to synthesize SAPO-5 catalysts which are highly active in catalyzing acylation of furan, surface modification of SAPO-5 is needed.

Several methods have been identified as the promising approaches to improve the surface acidity such as functionalization of organic acids [24], isomorphous substitution of heteroatoms [25–27], dealumination [28,29], impregnation [30] and post-synthesis treatments [30,31]. In particular, grafting of metal chlorides (e.g., GaCl_3 , FeCl_3 , AlCl_3) on solid supports have found to be an effective approach to enhance the surface acidity of the solid catalysts [32–36]. However, the metal chloride salts tend to leach out from the support during the catalytic reactions as weak chemical interactions are involved [37]. Furthermore, the effects of incorporation of metal chlorides on SAPO-5 for catalyzing acylation of furan are not known thus far and hence, comprehensive work on this study is worth to be further explored.

In this paper, we intend to study the influence of incorporation of metal chlorides (CoCl_2 , CuCl_2 , SnCl_4 , FeCl_3 , ZnCl_2) on the physico-chemical properties of SAPO-5 (topology, morphology, particle size, surface porosity and acidity). The incorporation of metal chlorides is performed using a simple grafting approach followed by additional thermochemical activation to induce strong chemical bondings between the metal chlorides and the SAPO-5 support. The catalytic behavior of the grafted SAPO-5 solids is then tested in the Friedel–Crafts acylation of 2-methylfuran under novel non-microwave instant heating conditions, and their catalytic performance and reusability are also compared with the conventional acid catalysts.

2. Experimental

2.1. Synthesis of 1-benzyl-2,3-dimethyl-1H-imidazol-3-ium hydroxide ([bzmIm]OH) Template Solution

Initially, 1,2-dimethylimidazole (30.00 g, 98%, Merck) and benzyl chloride (66.00 g, 99%, Merck) were dissolved in ethanol (40 mL, 99.7%, QRëc). The clear solution mixture was then refluxed at 100°C for 7 h under constant magnetic stirring rate (400 rpm). The resulting [bzmIm]Cl white solid product was washed with acetone for five times before drying at 80°C overnight. The dried [bzmIm]Cl ionic salt was then ion-exchanged with Amberlite® IRN-78 hydroxide resin (Sigma-Aldrich) in distilled water. After the ion exchange process, the resins were filtered and the solution was titrated with 0.1 M HCl solution to ensure 90% OH^- ion exchange was achieved. Finally, the [bzmIm]OH template solution was concentrated to 30.0 wt % prior further use.

2.2. Synthesis of SAPO-5 Molecular Sieve

The SAPO-5 microporous solid was synthesized under hydrothermal condition using a hydrogel system with a molar chemical composition of $1\text{Al}_2\text{O}_3:2.5\text{P}_2\text{O}_5:2.5[\text{bzmIm}]_2\text{O}:0.47\text{SiO}_2:180\text{H}_2\text{O}$. First, aluminum isopropoxide ($\text{Al}(\text{OiPr})_3$, 3.441 g, 98%, Sigma-Aldrich) and $[\text{bzmIm}]\text{OH}$ (28.000 g) were mixed in distilled water (6.224 g) and the mixture was magnetically stirred (400 rpm) for 40 min. Phosphoric acid (H_3PO_4 , 2.670 g, 85.5%, Sigma-Aldrich) was then slowly added into the mixture in a dropwise manner under continuous stirring where the entire process of addition took about 15 min. Subsequently, colloidal HS-40 silica (0.583 g, 40% SiO_2 , Sigma-Aldrich) was added to the hydrogel mixture. The resulting hydrogel was stirred for another 5 min before it was transferred to a 50-mL Teflon-lined stainless-steel autoclave for crystallization (180 °C, 10 h). After hydrothermal treatment, the solid product was recovered by filtration, washed with distilled water until pH 7 and freeze dried. Finally, the as-synthesized SAPO-5 was calcined at 550 °C for 6 h with a heating rate of 1 °C/min in order to remove the organic template.

2.3. Preparation of Metal Chlorides Grafted SAPO-5 ($\text{MCl}_x/\text{SAPO-5}$, $M = \text{Cu, Co, Sn, Fe, Zn}$) Solids

Five types of metal chlorides, namely CuCl_2 , AlCl_3 , CoCl_2 , FeCl_3 , ZnCl_2 , were grafted on SAPO-5 using the following procedure: Typically, the metal chloride in anhydrous form (0.5 mmol, Sigma-Aldrich) was first dissolved in ethanol (20 mL) at room temperature. The calcined SAPO-5 (1.500 g) was then added into the solution and the mixture was refluxed at 80 °C for 2 h. The solids were recovered by rotary evaporation at 80 °C, and heated at 300 °C for 3 h under air flow to produce the respective $\text{MCl}_x/\text{SAPO-5}$ solids where $M = \text{Cu, Co, Sn, Fe}$ and Zn (Figure 1).

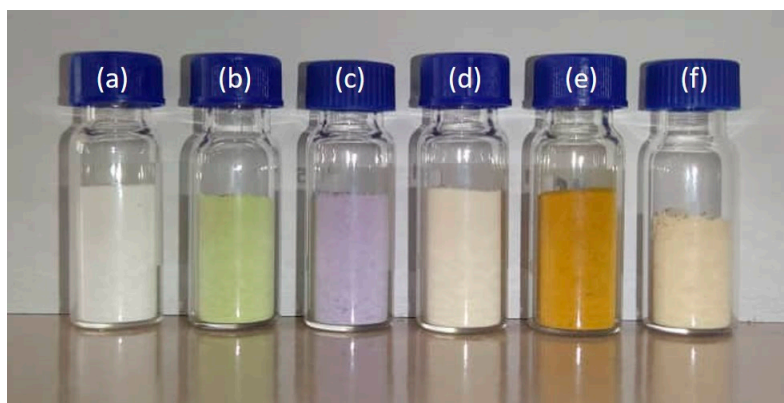


Figure 1. Physical appearance of (a) SAPO-5, (b) $\text{CuCl}_x/\text{SAPO-5}$, (c) $\text{CoCl}_x/\text{SAPO-5}$, (d) $\text{SnCl}_x/\text{SAPO-5}$, (e) $\text{FeCl}_x/\text{SAPO-5}$ and (f) $\text{ZnCl}_x/\text{SAPO-5}$.

2.4. Characterization

The phase purity of samples was examined by a Bruker Advance D8 XRD diffractometer ($\text{CuK}\alpha$ radiation, $\lambda = 1.5418 \text{ \AA}$, 40 kV, 10 mA) using a scan speed of $0.2^\circ/\text{min}$ and a step size of 0.02° . The d spacing in (100) plane (d_{100}) and unit cell parameters (a_0) of the solid samples were calculated using the Equations (1) and (2), respectively:

$$d_{100} = \frac{\lambda}{2 \sin \theta} \quad (1)$$

$$a_0 = \frac{2d_{100}}{\sqrt{3}} \quad (2)$$

The surface and morphological properties of the solids were studied using a JEOL JSM-6701F FESEM microscope while the micro-elemental analysis was performed by using an EDX spectrometer (Oxford Instruments Ltd., UK). The porous properties of the samples were studied using the nitrogen

adsorption-desorption analysis at $-196\text{ }^{\circ}\text{C}$. Prior to analysis, the powder sample (ca. 80 mg) was loaded in a Micromeritics ASAP 2010 analyzer (USA) and degassed under vacuum ($250\text{ }^{\circ}\text{C}$, 8 h). Brunauer–Emmett–Teller (BET) was then used to determine the surface area while the average pore diameter was estimated using the Barrett–Joyner–Halenda model. The surface acidity of the solids was examined by using pyridine adsorption combined with FTIR spectroscopy. Prior to analysis, a self-supported wafer (ca. 8 mg) was prepared and degassed in an IR vacuum cell at $300\text{ }^{\circ}\text{C}$ under vacuum (4 h, 10^{-6} bar). The background spectrum of the sample was acquired after cooling to room temperature. Subsequently, pyridine was adsorbed onto the sample for 1 min. The excessive pyridine was then evacuated, and the IR spectrum of the pellet was recorded (6 cm^{-1} resolution, 200 scans accumulation). The pellet was heated at $150\text{ }^{\circ}\text{C}$ and maintained for 1 h before the second IR spectrum was recorded after cooling. The pellet was further heated at $300\text{ }^{\circ}\text{C}$ for 1 h before the last IR spectrum was collected. The absorption bands due to Lewis and Brønsted acid sites were detected within the range of $1600\text{--}1400\text{ cm}^{-1}$ and the amount of both acid sites in the solid samples were calculated according to [38].

2.5. Catalytic Testing

The catalytic activity of $\text{MCl}_x/\text{SAPO-5}$ was studied on the Friedel–Crafts acylation of 2-methylfuran under novel non-microwave instant heating conditions, where acetic anhydride was used as an acylating agent. Initially, the activated catalyst (0.200 g, $200\text{ }^{\circ}\text{C}$, 1 h) was loaded in a glass reaction vessel before acetic anhydride (14.1 mmol) and 2-methylfuran (4.7 mmol) were successively added. The vessel was then sealed with a silicone rubber cap and instantly heated in an Anton Paar's Monowave 50 reactor ($110\text{ }^{\circ}\text{C}$, 20 min, 800 rpm stirring). After the reaction, the catalyst was recovered using high-speed centrifugation ($10,000 \times g$ rpm, 5 min) while the reaction solution was quantitatively and qualitatively analyzed using a gas chromatograph (Agilent 7890A, Equity-5 capillary column) and a gas chromatography-mass spectrometer (Agilent 7890A/5975C GCMS System, SPB-1 column), respectively, where toluene (5 μL) was added as an internal standard.

3. Results and Discussion

3.1. Characterization

The $\text{MCl}_x/\text{SAPO-5}$ catalysts ($\text{M} = \text{Cu}, \text{Co}, \text{Sn}, \text{Fe}$ or Zn) were synthesized by using a facile grafting method where the chloride salts were first dissolved in polar solvent before SAPO-5 solid support was added. The solvent was then removed via rotary evaporation before subjecting to thermochemical activation at $300\text{ }^{\circ}\text{C}$ to induce strong chemical bondings formation between the metal chlorides and the SAPO-5 support. In order to confirm this phenomenon, the $\text{MCl}_x/\text{SAPO-5}$ samples before and after thermochemical activation (0.200 g) were dispersed and sonicated in ethanol solution (5 mL) for 30 min. It was shown that for the non-thermochemical activated $\text{MCl}_x/\text{SAPO-5}$ samples, colored ethanol solutions were obtained after sonication indicating weak interaction between the metal chloride molecules and the SAPO-5 surface. As a result, a severe leaching problem of colored metal chloride salts was observed, and the results surprisingly were not in line with the works reported in [32,39]. However, the leaching problem was significantly suppressed after thermochemical activation, where the ethanol solutions remain almost transparent after sonication. Thus, it can be concluded that strong chemical bonding between metal chloride and SAPO-5 had been formed after thermochemical activation.

Figure 2 shows the XRD patterns of $\text{MCl}_x/\text{SAPO-5}$ solids and the XRD pattern of pristine SAPO-5 was also recorded for comparison purposes. The phase purity of SAPO-5 in all samples is evidenced from the XRD patterns where all major XRD peaks at 7.41° (100), 14.70° (200), 19.61° (210), 20.68° (002), 22.23° (211), 25.84° (220) and 24.38° (410) are observed, and they are well indexed according to the standard hexagonal AFI crystal phase with space group $p6/mmc$ [40]. As compared to pristine SAPO-5, the XRD peaks of $\text{MCl}_x/\text{SAPO-5}$ are slightly right-shifted which can be explained by the reduction of micropore sizes of SAPO-5 as a result of the grafting of metal chloride species [41]. This observation can

also be proven based on the reduction of the XRD peaks intensity of $MCl_x/SAPO-5$ after the grafting process. Furthermore, no additional XRD peaks are seen in all $MCl_x/SAPO-5$ samples indicating that the metal chloride particles are homogeneously distributed on the surface of SAPO-5.

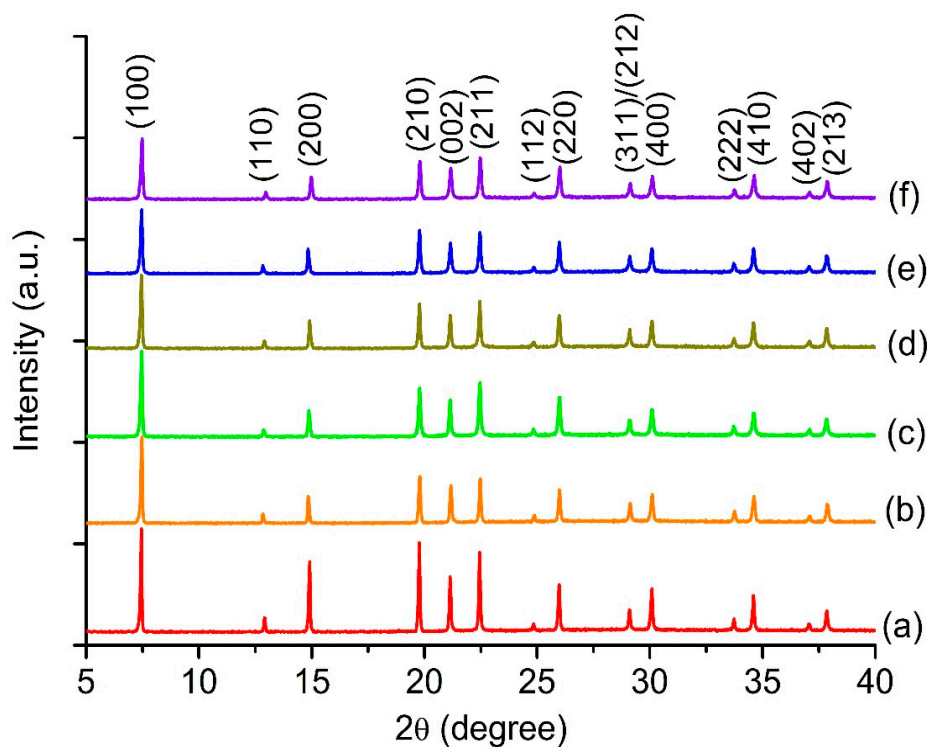


Figure 2. XRD patterns of (a) pristine SAPO-5, (b) $CuCl_x/SAPO-5$, (c) $CoCl_x/SAPO-5$, (d) $SnCl_x/SAPO-5$, (e) $FeCl_x/SAPO-5$ and (f) $ZnCl_x/SAPO-5$.

The effects of incorporation of metal chlorides on the morphological properties of SAPO-5 were studied using the FESEM microscopy technique. Figure 3 displays the FESEM images of pristine SAPO-5 and $MCl_x/SAPO-5$ crystals. As shown, all samples exhibit hexagonal prisms similar to the theoretical shape [42,43], and the morphology of the samples remains intact indicating that the structural integrity of SAPO-5 is preserved after grafting modification and thermochemical activation. The particle size distribution based on the length of the hexagonal prisms of all samples is also plotted by measuring the length of 100 single crystal particles at different spots. The statistical results indicate that the pristine SAPO-5 is sized ranging from 75 nm to 560 nm and has an average crystal size of 228 nm. Upon grafting of metal chloride compounds, the crystal size distribution is nearly intact, and the average crystal size remains almost identical (~230 nm). Furthermore, no big granulate particles of metal chlorides are observed on the surface of $MCl_x/SAPO-5$ crystals revealing that no agglomeration of metal chloride salts occurs, and they are evenly distributed on the support surface; this is in accordance with the XRD observation (Figure 2).

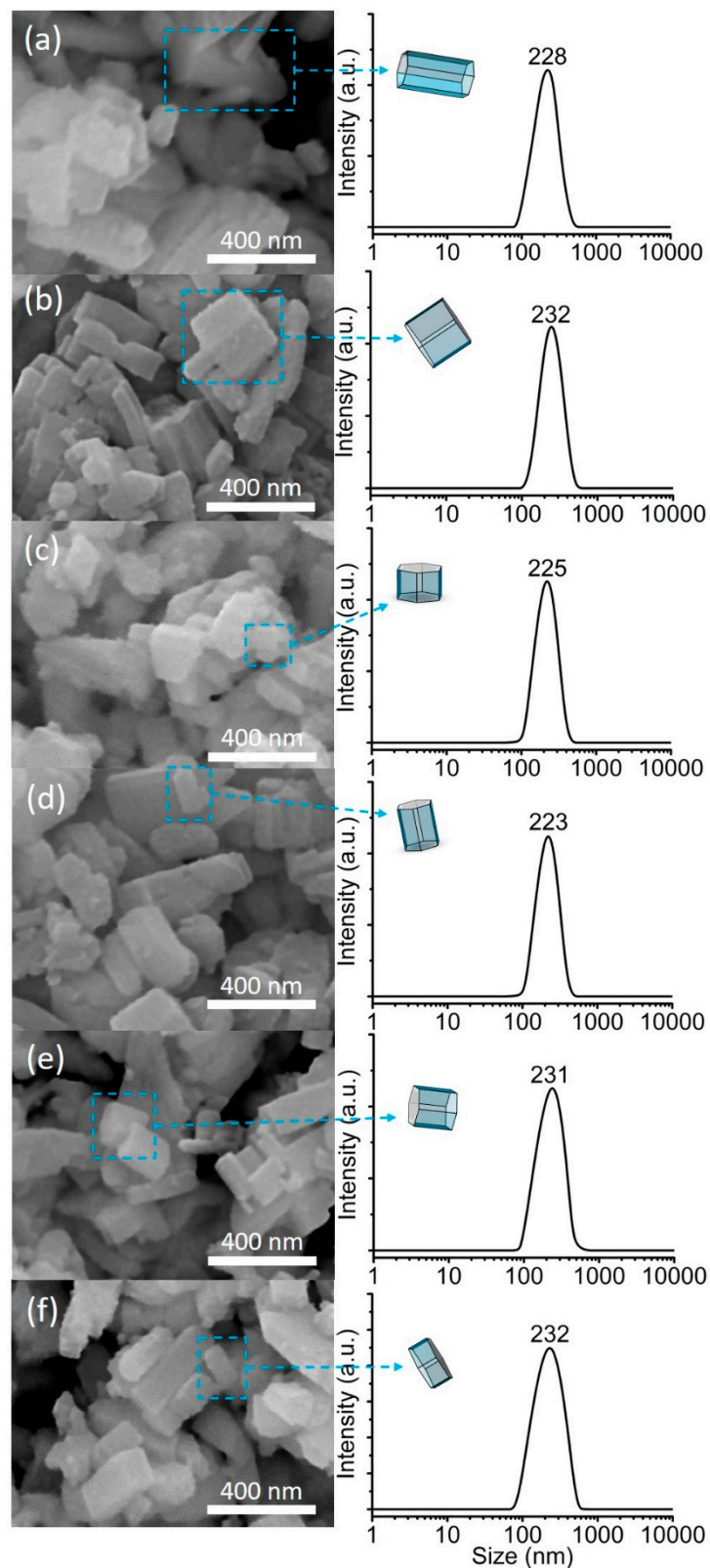


Figure 3. SEM images and crystal size distributions based on the length of the hexagonal prisms of (a) pristine SAPO-5, (b) $\text{CuCl}_x/\text{SAPO-5}$, (c) $\text{CoCl}_x/\text{SAPO-5}$, (d) $\text{SnCl}_x/\text{SAPO-5}$, (e) $\text{FeCl}_x/\text{SAPO-5}$ and (f) $\text{ZnCl}_x/\text{SAPO-5}$. The selected hexagonal prism crystals in each sample are also highlighted and compared with the theoretical ones.

The chemical compositions of pristine SAPO-5 and MCl_x /SAPO-5 are confirmed by using EDX spectroscopy, micro-elemental analysis and the amount of each element in the samples is summarized in Table 1. As calculated, the molecular formula of pristine SAPO-5 is $Si_{1.485}Al_{12.093}P_{10.196}O_{47.858}$ which is quite similar to the theoretical molecular formula of AFI-type molecular sieve ($Si_nAl_{12}P_{12-n}O_{48}$) (Table 2) [38]. The Si/(P + Al + Si) ratio of pure SAPO-5 is calculated to be 0.062, where the presence of Si atoms is the attribution to the generation of surface Brönsted acidity in SAPO-5 [44]. Meanwhile, the molecular formulae of $CuCl_x$ /SAPO-5, $CoCl_x$ /SAPO-5, $SnCl_x$ /SAPO-5, $FeCl_x$ /SAPO-5 and $ZnCl_x$ /SAPO-5 are determined to be $Cu_{3.019}Cl_{5.826}Si_{1.419}Al_{11.843}P_{10.486}O_{47.926}$, $Co_{2.957}Cl_{5.825}Si_{1.455}Al_{12.012}P_{10.281}O_{47.817}$, $Sn_{2.916}Cl_{3.576}Si_{1.464}Al_{11.993}P_{10.221}O_{47.827}$, $Fe_{3.039}Cl_{4.825}Si_{1.455}Al_{12.210}P_{10.098}O_{47.838}$ and $Zn_{2.945}Cl_{3.535}Si_{1.369}Al_{12.159}P_{10.252}O_{47.865}$, respectively, where the Si/(P+Al+Si) ratio remains intact (~0.061) after surface grafting treatment.

The amount of metal and chloride atoms present in SAPO-5 is also determined. Interestingly, $ZnCl_x$ /SAPO-5, $FeCl_x$ /SAPO-5 and $SnCl_x$ /SAPO-5 displayed lower Cl:M ratio than their respective pure metal chloride salts. Hence, the elemental analysis suggests that the metal chlorides have been incorporated onto the surface of $ZnCl_x$ /SAPO-5, $FeCl_x$ /SAPO-5 and $SnCl_x$ /SAPO-5 via condensation reaction ($AFI-OH + Cl-M \rightarrow AFI-O-M + HCl$). In contrast, $CoCl_x$ /SAPO-5 and $CuCl_x$ /SAPO-5 show Cl:M ratio ≈ 2 , which is nearly similar to their respective metal salts. Hence, the study demonstrates that no condensation reaction between AFI-OH and Cl-M took place in $CoCl_x$ /SAPO-5 and $CuCl_x$ /SAPO-5. Instead, we believe that the $CoCl_2$ and $CuCl_2$ are bound to the SAPO-5 surface via dative covalent bondings, where Cu^{2+} and Co^{2+} cations are able to form four to six chemical bondings (covalent and dative bonds) [45,46].

The possible structures of MCl_x /SAPO-5 are shown in Figure 4 after spectroscopy investigations are considered. For $CoCl_x$ /SAPO-5 and $CuCl_x$ /SAPO-5, the metal chloride molecules are bound to the surface of SAPO-5 via dative bondings where these bonds are not as strong as covalent bondings (Figure 4b,c). In contrast, the metal chloride molecules are covalently bound to the surface of SAPO-5 in $SnCl_x$ /SAPO-5, $FeCl_x$ /SAPO-5 and $ZnCl_x$ /SAPO-5, where the Cl atom(s) of the respective metal chloride is/are condensed together with the O-H group of the SAPO-5 defect sites (Figure 4d–f).

Table 1. Chemical compositions of metal chlorides supported on SAPO-5.

Element	Samples (wt%)					
	SAPO-5	$CuCl_x$ /SAPO-5	$CoCl_x$ /SAPO-5	$SnCl_x$ /SAPO-5	$FeCl_x$ /SAPO-5	$ZnCl_x$ /SAPO-5
C	18.47	42.15	39.86	5.14	17.14	23.10
O	39.63	21.36	20.20	35.92	34.01	30.90
Al	16.90	8.91	8.42	15.20	14.65	13.25
Si	2.16	1.11	1.05	1.93	1.81	1.55
P	16.36	9.05	8.56	14.87	13.91	12.82
Cl	-	5.76	5.45	5.96	7.61	5.06
Cu	-	5.34	-	-	-	-
Pt	6.49	6.32	5.98	4.73	3.31	5.13
Co	-	-	5.05	-	-	-
Sn	-	-	-	16.24	-	-
Fe	-	-	-	-	7.54	-
Zn	-	-	-	-	-	7.77
Total	100	100	100	100	100	100

Table 2. Calculated molecular formulae and elemental ratios of metal chlorides supported on SAPO-5.

Sample	Molecular Formula	Si/(Al + P + Si) Ratio	Cl/M Ratio ^a
SAPO-5	Si _{1.485} Al _{12.093} P _{10.196} O _{47.858}	0.062	-
CuCl _x /SAPO-5	Cu _{3.019} Cl _{5.826} Si _{1.419} Al _{11.843} P _{10.486} O _{47.926}	0.060	1.93 (2)
CoCl _x /SAPO-5	Co _{2.957} Cl _{5.825} Si _{1.455} Al _{12.012} P _{10.281} O _{47.817}	0.061	1.97 (2)
SnCl _x /SAPO-5	Sn _{2.916} Cl _{3.576} Si _{1.464} Al _{11.993} P _{10.221} O _{47.827}	0.062	1.23 (4)
FeCl _x /SAPO-5	Fe _{3.039} Cl _{4.825} Si _{1.455} Al _{12.210} P _{10.098} O _{47.838}	0.061	1.59 (3)
ZnCl _x /SAPO-5	Zn _{2.945} Cl _{3.535} Si _{1.369} Al _{12.159} P _{10.252} O _{47.865}	0.059	1.20 (2)

^a The brackets show the actual Cl/M ratio of the respective pure metal chloride salts.

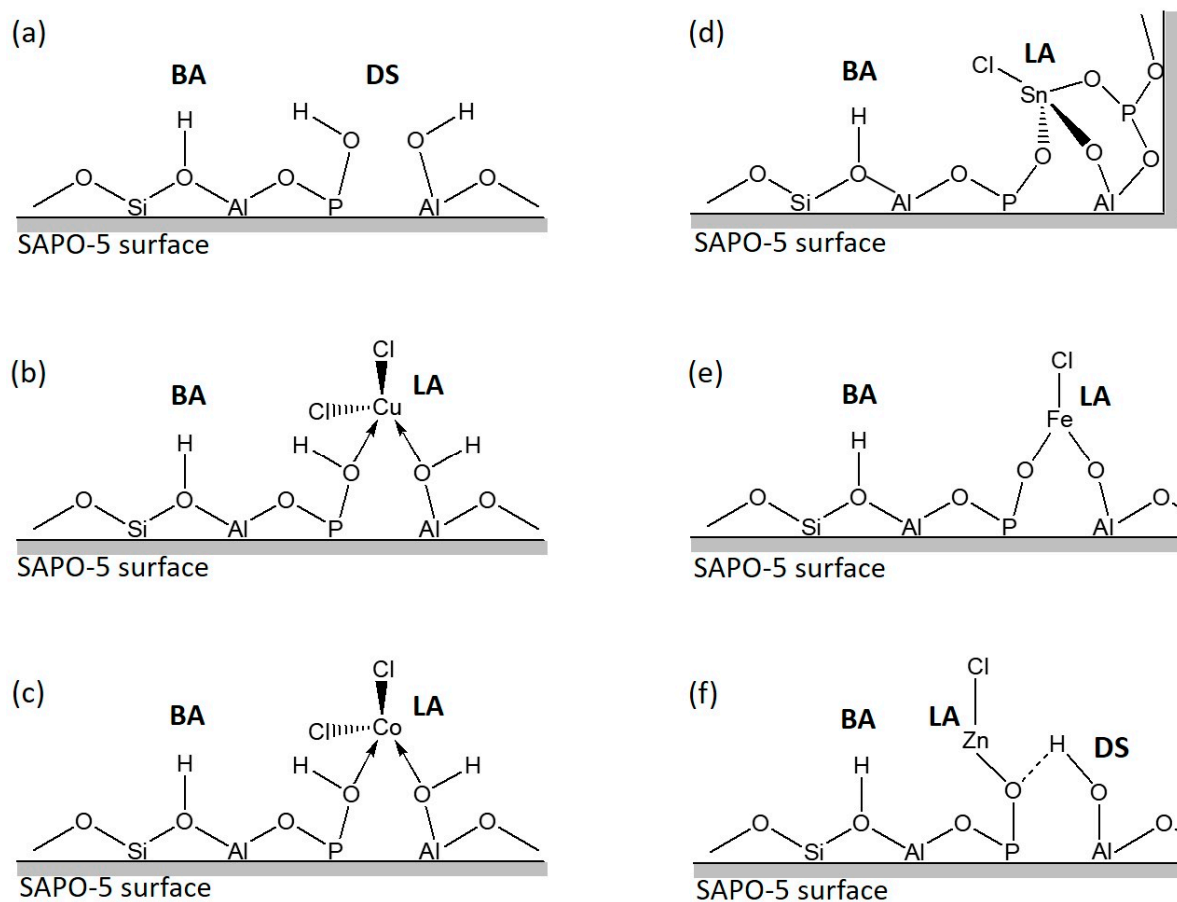


Figure 4. Possible structures of (a) SAPO-5, (b) CuCl_x/SAPO-5, (c) CoCl_x/SAPO-5, (d) SnCl_x/SAPO-5, (e) FeCl_x/SAPO-5 and (f) ZnCl_x/SAPO-5 where the Brønsted acid, Lewis acid and defect sites are denoted as BA, LA and DS, respectively. The arrow and dot line represent the dative and hydrogen bondings, respectively.

The porous properties of pristine SAPO-5 and MCl_x/SAPO-5 solids were studied using XRD and N₂ adsorption-desorption analyses, and the data are summarized in Table 3. The study shows that the pristine SAPO-5 initially has a specific BET surface area (S_{BET}) and an average pore size (D) of 257 m²/g and 37.9 nm, respectively. It also exhibits a considerably high total pore volume (0.35 cm³/g) due to its highly porous nature. After incorporating various metal chlorides, all grafted solid samples show a decrease in the surface area, pore size and pore volume where ZnCl_x/SAPO-5 experiences the most significant effects with those parameters reduce to 89 m²/g, 19.3 nm and 0.04 cm³/g, respectively. Hence, this phenomenon reveals that the metal chloride particles are partially filled and occupied the pores in MCl_x/SAPO-5, which is in agreement with the XRD results that show a decrease of d_{100} spacing and unit cell parameters upon grafting modification (Figure 2 and Table 3).

Table 3. Textural and surface properties of $MCl_x/SAPO-5$ solids.

Samples	d_{100} Spacing (Å)	a_0 (Å) ^a	S_{BET} (m ² /g) ^b	D (nm) ^c	V_{tot} (cm ³ /g) ^d
SAPO-5	11.95	13.80	257	37.9	0.35
CuCl _x /SAPO-5	11.84	13.67	130	26.7	0.16
CoCl _x /SAPO-5	11.85	13.68	122	24.7	0.07
SnCl _x /SAPO-5	11.86	13.69	107	23.3	0.09
FeCl _x /SAPO-5	11.85	13.68	115	26.1	0.12
ZnCl _x /SAPO-5	11.82	13.65	89	19.3	0.04

^a Unit cell parameter; ^b Specific BET surface area; ^c Average pore diameter; ^d Total pore volume.

The surface acidity of $MCl_x/SAPO-5$ was characterized by pyridine adsorption coupled with FTIR spectroscopy, viz. a very reliable analysis for surface acidity study (type, strength and amount of acid sites). By using FTIR spectroscopy, the Lewis acid sites and Brönsted acid sites of a solid acid catalyst can be detected at 1454 and 1545 cm⁻¹, respectively [47]. The pyridine adsorption-FTIR spectra after desorption at 25 °C, 150 °C and 300 °C are shown in Table 4 where these three desorption temperatures can be used to identify weak, mild and strong acid sites. For pristine SAPO-5, the Brönsted acid sites with strong acid strength (~25 µmol/g) are observed, while mild Lewis acidity (~72 µmol/g) due to surface defect sites is also detected.

Upon grafting of metal chlorides, the Lewis acidity of $MCl_x/SAPO-5$ is significantly enhanced while the Brönsted acidity remains almost unaffected. For instance, the mild and strong Lewis acidities of FeCl_x/SAPO-5 have increased about 4 and 25 folds after surface modification, respectively. Among the $MCl_x/SAPO-5$ samples prepared, ZnCl_x/SAPO-5, which has the lowest surface area, possesses the largest number of Lewis acid sites especially with mild acid strength (444.9 µmol/g) whereas FeCl_x/SAPO-5 has the largest amount of strong Lewis acid sites (219.1 µmol/g). On the other hand, CuCl_x/SAPO-5 possesses the lowest number of mild and strong Lewis acid sites; only 126.6 and 38.9 µmol/g were measured, respectively.

The Lewis–Brönsted acids ratios (L/B) are also calculated in order to reveal the acid nature of the solids. For pristine SAPO-5, the L/B ratio with mild acid strength is very low (2.7) while the L/B ratio for strong acid strength is merely 0.3. Hence, the results agree with the previous work that SAPO-5 is a mild-to-strong Brönsted acid solid catalyst [48]. Interestingly, the L/B ratio increases significantly after incorporation of metal chlorides, particularly ZnCl_x/SAPO-5 and FeCl_x/SAPO-5, where the Lewis acidity with mild and strong acid strength dominates the total acid sites of the samples.

Table 4. Surface acidity of $MCl_x/SAPO-5$ measured using pyridine (Py) adsorption coupled with FTIR spectroscopy technique.

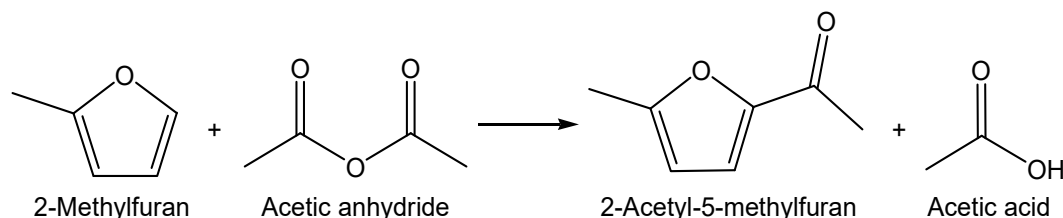
Samples	Py-FTIR Acidity (µmol/g)											
	Lewis Acid Sites (L)			Brönsted Acid Sites (B)			Total Acid Sites (L + B)			L/B Ratio		
	25 °C	150 °C	300 °C	25 °C	150 °C	300 °C	25 °C	150 °C	300 °C	25 °C	150 °C	300 °C
SAPO-5	432.4	71.9	8.6	33.6	26.2	24.6	466.0	98.1	33.2	12.9	2.7	0.3
CuCl _x /SAPO-5	370.6	126.6	38.9	34.0	28.1	24.6	404.6	154.7	63.5	10.9	4.5	1.6
CoCl _x /SAPO-5	322.5	137.4	100.9	33.8	27.2	25.1	356.3	164.6	126.0	9.5	5.1	4.0
SnCl _x /SAPO-5	320.9	167.3	148.9	32.3	25.4	23.7	353.2	192.7	172.6	9.9	6.6	6.3
FeCl _x /SAPO-5	534.1	290.8	219.1	31.4	26.2	25.2	565.5	317.0	244.3	17.0	11.1	8.7
ZnCl _x /SAPO-5	496.8	444.9	83.5	31.2	27.7	22.8	528.0	472.6	106.3	15.9	16.1	3.7

3.2. Catalytic Testing

3.2.1. Effect of Reaction Time and Temperature

Friedel–Crafts acylation of 2-methylfuran with acetic anhydride as an acylation agent was selected as a model reaction (Scheme 1) to study the catalytic behavior of MCl_x /SAPO-5 catalysts. The reaction was conducted at 90–110 °C within 20 min by using an instant heating technique that mimics microwave fast heating [49]. Of note, the reaction condition used is much gentler than those reported in [50–53].

The reaction is inactive in the absence of a catalyst (110 °C, 20 min) where nearly no reaction conversion (0.2%) was recorded (Figure 5). When MCl_x /SAPO-5 catalysts are added, the conversion increases tremendously with 100% selective to 2-acetyl-5-methylfuran, viz. a valuable biofuel compound and intermediate in the pharmaceutical industry [54], under similar reaction conditions (110 °C, 20 min). Among the solid catalysts prepared, $ZnCl_x$ /SAPO-5 is the most reactive, giving 94.5% conversion, followed by $FeCl_x$ /SAPO-5 (87.8%), $SnCl_x$ /SAPO-5 (81.5%), $CoCl_x$ /SAPO-5 (72.3%) and $CuCl_x$ /SAPO-5 (66.7%). Hence, the catalytic reaction results further support the FTIR-pyridine adsorption study that the acylation of 2-methylfuran requires mild-to-strong Lewis acidity to accelerate the reaction. The catalytic reaction was also tested with pristine SAPO-5. However, only 45.1% conversion was afforded under similar reaction conditions due to its low Lewis acidity.



Scheme 1. Friedel-Crafts acylation of 2-methylfuran with acetic anhydride.

The activation energies of acylation of a 2-methylfuran reaction catalyzed with and without MCl_x /SAPO-5 solid catalysts are also determined using the Arrhenius plots in order to understand the chemical kinetics of this reaction. The reaction was found to follow second-order rate law where the reaction kinetics depend on the concentrations of 2-methylfuran and acetic anhydride reactants [55]. The second-order rate constants, k_{2nd} , at 90 °C, 100 °C and 110 °C are obtained and used to plot the Arrhenius linear plot: $\ln k$ versus $1/T$. The activation energy of non-catalyzed acylation of 2-methylfuran is very high ($181.3 \text{ kJ mol}^{-1}$) [49]. Nevertheless, the activation energy is reduced when pristine SAPO-5 or MCl_x /SAPO-5 solid catalysts are added (Figure 6). This phenomenon occurs because the solid acid catalyst has increased the rate of reaction by offering an alternative route to the reaction product which is more feasibly occurred (lower activation energy) than the reaction pathway not mediated by the catalyst [56]. Among the solid acid catalysts studied, $ZnCl_x$ /SAPO-5 gives the lowest activation energy (36.4 kJ mol^{-1}), followed by $FeCl_x$ /SAPO-5 (39.2 kJ mol^{-1}), $SnCl_x$ /SAPO-5 (40.1 kJ mol^{-1}), $CoCl_x$ /SAPO-5 (63.9 kJ mol^{-1}), $CuCl_x$ /SAPO-5 (82.3 kJ mol^{-1}) and SAPO-5 (96.4 kJ mol^{-1}). Based on the catalytic study results, the best catalyst is $ZnCl_x$ /SAPO-5 and hence it is chosen for further catalytic study.

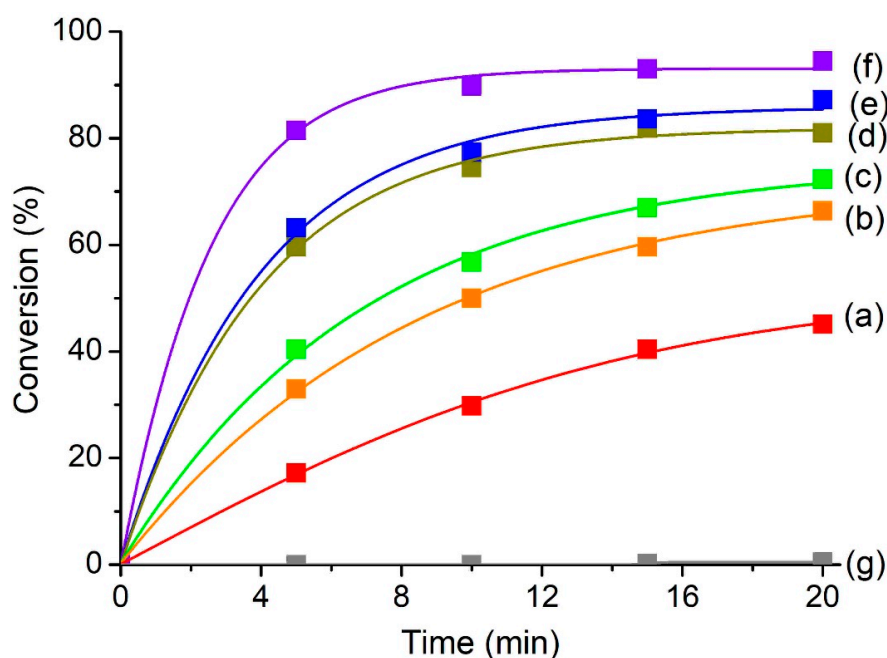


Figure 5. Acylation of 2-methylfuran catalyzed by (a) SAPO-5, (b) CuCl_x/SAPO-5, (c) CoCl_x/SAPO-5, (d) SnCl_x/SAPO-5, (e) FeCl_x/SAPO-5 and (f) ZnCl_x/SAPO-5 at 110 °C. Reaction conditions: Catalyst = 0.20 g, 2-methylfuran = 4.7 mmol, acetic anhydride = 14.1 mmol, solvent-free. The reaction without adding any catalyst is shown in (g).

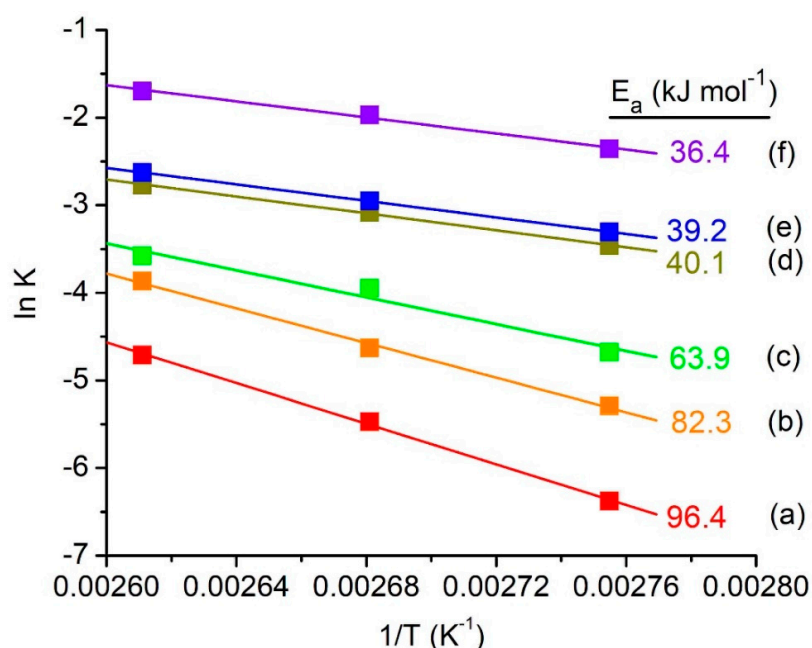


Figure 6. The Arrhenius linear plots and activation energies (E_a) of acylation of 2-methylfuran catalyzed by (a) pristine SAPO-5, (b) CuCl_x/SAPO-5, (c) CoCl_x/SAPO-5, (d) SnCl_x/SAPO-5, (e) FeCl_x/SAPO-5 and (f) ZnCl_x/SAPO-5. Reaction conditions: Catalyst = 0.20 g, 2-methylfuran = 4.7 mmol, acetic anhydride = 14.1 mmol, reaction temperature: 90, 100 and 110 °C, time = 0–20 min, solvent-free.

3.2.2. Catalytic Comparative Study

The catalytic performance of MCl_x/SAPO-5 is also compared with some common homogeneous Lewis and Brønsted acid catalysts under the same reaction condition where an equivalent amount

of catalyst is applied. As shown in Table 5, homogeneous Lewis acids, such as ZnCl_2 (75.5%) and FeCl_3 (68.1%), are found to be more reactive than the homogeneous Brønsted acids, such as H_2SO_4 (68.4%), HNO_3 (56.2%) and CH_3COOH (32.7%), where the former class of catalysts undergoes different catalytic reaction route but kinetically more favored by first dissociating the C-O-C bond of the anhydride into the acetoxy anion (limiting step) instead of acylium cation (by the latter ones) prior to forming 2-acetyl-5-methylfuran [54]. Nevertheless, these homogeneous catalysts are not reusable due to separation difficulty and surprisingly, their catalytic reactivity is much lower than those of $\text{SnCl}_x/\text{SAPO-5}$, $\text{FeCl}_x/\text{SAPO-5}$ and $\text{ZnCl}_x/\text{SAPO-5}$. Hence, it is speculated that the presence of both Brønsted and Lewis acid sites in the $\text{MCl}_x/\text{SAPO-5}$ might contribute to the synergistic cooperative effect on the catalytic enhancement of the Friedel–Crafts reaction [57].

Table 5. Catalytic comparison study between $\text{MCl}_x/\text{SAPO-5}$ and some common homogeneous catalysts in acylation of 2-methylfuran ^a.

Catalyst	Conversion (%)
SAPO-5	45.1
$\text{CuCl}_x/\text{SAPO-5}$	66.7
$\text{CoCl}_x/\text{SAPO-5}$	72.3
$\text{SnCl}_x/\text{SAPO-5}$	81.5
$\text{FeCl}_x/\text{SAPO-5}$	87.8
$\text{ZnCl}_x/\text{SAPO-5}$	94.5
H_2SO_4	68.4
CH_3COOH	32.7
HNO_3	56.2
ZnCl_2	75.7
FeCl_3	68.1

^a Reaction conditions: Catalyst = 0.20 g or equivalent to 110 μmol homogeneous catalyst, 2-methylfuran = 4.7 mmol, acetic anhydride = 14.1 mmol, solvent-free, reaction temperature = 110 °C, time = 20 min.

3.2.3. Catalyst Reusability Test

Catalyst reusability of $\text{MCl}_x/\text{SAPO-5}$ catalysts is also studied for four consecutive cycles as it represents a significant advantage for green chemical production [57]. As shown in Figure 7, $\text{SnCl}_x/\text{SAPO-5}$, $\text{FeCl}_x/\text{SAPO-5}$ and $\text{ZnCl}_x/\text{SAPO-5}$, which have stronger covalently-bonded metal chlorides, exhibit fewer steep slopes than the $\text{CoCl}_x/\text{SAPO-5}$, and $\text{CuCl}_x/\text{SAPO-5}$, which have weaker dative bondings bound to the metal chloride compounds. As a result, the previous three catalysts have higher catalyst reusability than the latter two. Among the catalysts prepared, $\text{ZnCl}_x/\text{SAPO-5}$ is the most reactive and its reaction conversion remains considerably high (78.4%) even after the fourth consecutive run, whereas $\text{CoCl}_x/\text{SAPO-5}$ and $\text{CuCl}_x/\text{SAPO-5}$ show the least catalytic activity, where, their reaction conversion is almost comparable as that of pristine SAPO-5 after the fourth consecutive cycle. Thus, $\text{ZnCl}_x/\text{SAPO-5}$ is considerably stable in terms of catalyst reusability and hence, it can be a recyclable and active heterogeneous catalyst for various acid-catalyzed reactions.

Furthermore, the catalytic activity of metal chlorides leached in reaction solutions was also examined. The $\text{MCl}_x/\text{SAPO-5}$ (0.20 g) was first stirred in acetic anhydride (14.1 mmol) and 2-methyl furan (4.7 mmol) for 5 h at room temperature before the solution (after separated from the solid catalyst (10,000 rpm, 5 min)) was heated at 110 °C for 20 min. It is shown that the reaction conversions of the solutions after separating from $\text{ZnCl}_x/\text{SAPO-5}$, $\text{FeCl}_x/\text{SAPO-5}$ and $\text{SnCl}_x/\text{SAPO-5}$ (<5%) are lower than those of $\text{CoCl}_x/\text{SAPO-5}$ and $\text{CuCl}_x/\text{SAPO-5}$ (~10%). Thus, it indicates that the respective metal chlorides are strongly bound to the former three catalysts as compared to the latter two catalysts, in line with the XRD and ICP-OES spectroscopy data.

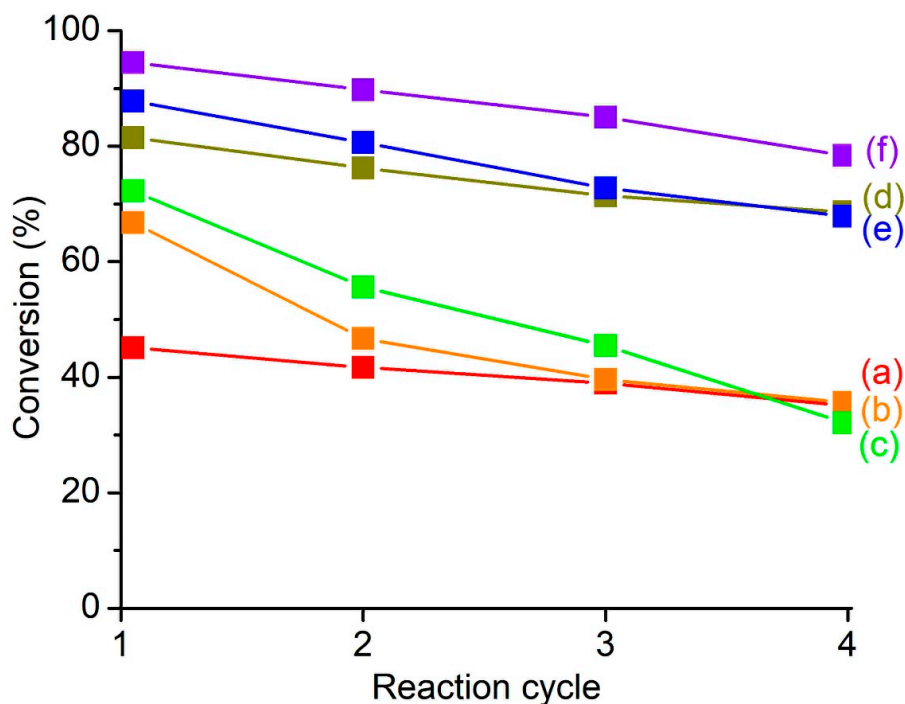


Figure 7. Reusability test of (a) SAPO-5, (b) $\text{CuCl}_x/\text{SAPO-5}$, (c) $\text{CoCl}_x/\text{SAPO-5}$, (d) $\text{SnCl}_x/\text{SAPO-5}$, (e) $\text{FeCl}_x/\text{SAPO-5}$ and (f) $\text{ZnCl}_x/\text{SAPO-5}$ for consecutive five reaction cycles. Reaction conditions: temperature = 110 °C, time = 20 min, 2-methylfuran = 4.7 mmol, acetic anhydride = 14.1 mmol, catalyst = 0.20 g $\text{MCl}_x/\text{SAPO-5}$.

4. Conclusions

In conclusion, metal chloride grafted on SAPO-5, $\text{MCl}_x/\text{SAPO-5}$ ($\text{M} = \text{Cu}, \text{Co}, \text{Sn}, \text{Fe}$ and Zn) have successfully been prepared. The elemental microanalysis results indicate that the thermochemical treatment is essential after grafting steps to foster the formation of chemical bondings between MCl_x and SAPO-5. It is found that Si–O–M covalent bonds are formed in $\text{ZnCl}_x/\text{SAPO-5}$, $\text{SnCl}_x/\text{SAPO-5}$ and $\text{FeCl}_x/\text{SAPO-5}$, whereas only dative bondings are formed in $\text{CoCl}_x/\text{SAPO-5}$ and $\text{CuCl}_x/\text{SAPO-5}$. In addition, the d_{100} spacing, surface area, average pore diameter and pore volume of $\text{MCl}_x/\text{SAPO-5}$ samples also decrease due to the deposition of MCl_x species on the supports' surface. The type of metal chlorides grafted is also found to have positive effects on the surface acidity and catalytic behavior of $\text{MCl}_x/\text{SAPO-5}$. $\text{ZnCl}_x/\text{SAPO-5}$, which has the lowest surface area, possesses the largest amount of mild-to-strong Lewis acid sites (472.6 $\mu\text{mol/g}$, L/B ratio = 16.1). As a result, it shows the best catalytic performance (94.5% conversion, 100% selective to 2-acetyl-5-methylfuran) under non-microwave instant heating condition (110 °C, 20 min), followed by $\text{FeCl}_x/\text{SAPO-5}$ (317.0 $\mu\text{mol/g}$, L/B ratio = 11.1, conversion = 87.8%), $\text{SnCl}_x/\text{SAPO-5}$ (192.7 $\mu\text{mol/g}$, L/B ratio = 6.6, conversion = 81.5%), $\text{CoCl}_x/\text{SAPO-5}$ (164.6 $\mu\text{mol/g}$, L/B ratio = 5.1, conversion = 72.3%), $\text{CuCl}_x/\text{SAPO-5}$ (154.7 $\mu\text{mol/g}$, L/B ratio = 4.5, conversion = 66.7%) and pristine SAPO-5 (98.1 $\mu\text{mol/g}$, L/B ratio = 2.7, conversion 45.1%). Most importantly, the performance of $\text{MCl}_x/\text{SAPO-5}$, particularly $\text{SnCl}_x/\text{SAPO-5}$, $\text{FeCl}_x/\text{SAPO-5}$ and $\text{ZnCl}_x/\text{SAPO-5}$, are more superior than the common homogeneous acid catalysts (H_2SO_4 , HNO_3 , CH_3COOH , FeCl_3 , ZnCl_2) with higher product conversion and catalyst reusability, offering new environment-friendly process with a facile catalyst separation.

Author Contributions: I.A.A.: Performed most of the experiments, wrote the manuscript. K.-L.W.: Give idea for the entire project, supervision, proofread the manuscript. T.C.L.: Applied for research funding, proofread the manuscript. B.S.O.: Give idea for the entire project, ran SEM investigation, proof-read the manuscript. E.-P.N.: Applied for research funding, conceived the entire project, wrote and proof-read the manuscript, supervision. All authors have read and agreed to the published version of the manuscript.

Funding: The financial support from USM Bridging Fund (304/PKIMIA/6316506) and FRGS (203/PKIMIA/6711642) grant are gratefully acknowledged. I.A. Auwal would also like to thank the USM Fellowship and TETFund for the scholarship provided.

Conflicts of Interest: The authors declare no conflict of interest.

References

1. Look, S.A.; Burch, M.T.; Fenical, W.; Zheng, Q.; Clardy, J. Kallolide A, a new antiinflammatory diterpenoid, and related lactones from the Caribbean octocoral *Pseudopterogorgia kallos* (Bielschowsky). *J. Org. Chem.* **1985**, *50*, 5741–5746. [[CrossRef](#)]
2. Schenkel, D.; Lemfack, M.C.; Piechulla, B.; Splivallo, R. A meta-analysis approach for assessing the diversity and specificity of belowground root and microbial volatiles. *Front. Plant Sci.* **2015**, *6*, 707. [[CrossRef](#)] [[PubMed](#)]
3. Banerjee, R.; Kumar, H.; Banerjee, M. Medicinal significance of furan derivatives: A Review. *Int. J. Rev. Life Sci.* **2012**, *2*, 7–16.
4. Harrison, I.T.; Lewis, B.; Nelson, P.; Rooks, W.; Roszkowski, A.; Tomolonis, A.; Fried, J.H. Nonsteroidal antiinflammatory agents. I. 6-substituted 2-naphthylacetic acids. *J. Med. Chem.* **1970**, *13*, 203–205. [[CrossRef](#)] [[PubMed](#)]
5. Li, Y.; Li, H.; Chen, H.; Wan, Y.; Li, N.; Xu, Q.; He, J.; Chen, D.; Wang, L.; Lu, J. Controlling crystallite orientation of diketopyrrolopyrrole-based small molecules in thin films for highly reproducible multilevel memory device: Role of furan substitution. *Adv. Funct. Mater.* **2015**, *25*, 4246–4254. [[CrossRef](#)]
6. Kruse, L.I.; Ladd, D.L.; Harsch, P.B.; McCabe, F.L.; Mong, S.M.; Faucette, L.; Johnson, R. Synthesis, tubulin binding, antineoplastic evaluation, and structure-activity relationship of oncodazole analogs. *J. Med. Chem.* **1989**, *32*, 409–417. [[CrossRef](#)]
7. Finan, P.; Fothergill, G. 506. Furans. Part II. Friedel-Crafts acylation of furan, 2-methylfuran, and 3-methylfuran. *J. Chem. Soc.* **1963**, 2723–2727. [[CrossRef](#)]
8. Spurlock, J.J. Hydantoinas as anticonvulsants. I. 5-R-5-(2-Thienyl)-hydantoinas. *J. Am. Chem. Soc.* **1953**, *75*, 1115–1117. [[CrossRef](#)]
9. Katritzky, A.R.; Suzuki, K.; Singh, S.K. C-acylation of 2-methylfuran and thiophene using N-acylbenzotriazoles. *Croat. Chem. Acta* **2004**, *77*, 175–178. [[CrossRef](#)]
10. Kresnawahjuesa, O.; Gorte, R.J.; White, D. The acylation of propene by acetic acid over H-[Fe] ZSM-5 and H-[Al] ZSM-5. *J. Mol. Catal. A Chem.* **2004**, *212*, 309–314. [[CrossRef](#)]
11. Blaser, H.-U.; Indolese, A.; Schnyder, A.; Steiner, H.; Studer, M. Supported palladium catalysts for fine chemicals synthesis. *J. Mol. Catal. A Chem.* **2001**, *173*, 3–18. [[CrossRef](#)]
12. Métivier, P. Catalysis for fine chemicals: An industrial perspective. In *Studies in Surface Science and Catalysis*; Elsevier: Amsterdam, The Netherlands, 2000; Volume 130, pp. 167–176.
13. Ng, E.-P.; Awala, H.; Komaty, S.; Mintova, S. Microwave-Green synthesis of AlPO-n and SAPO-n (n = 5 and 18) nanosized crystals and their assembly in layers. *Microporous Mesoporous Mater.* **2019**, *280*, 256–263. [[CrossRef](#)]
14. Wong, S.-F.; Deekomwong, K.; Wittayakun, J.; Ling, T.C.; Muraza, O.; Adam, F.; Ng, E.-P. Crystal growth study of KF nanozeolite and its catalytic behavior in Aldol condensation of benzaldehyde and heptanal enhanced by microwave heating. *Mater. Chem. Phys.* **2017**, *196*, 295–301. [[CrossRef](#)]
15. Ng, E.-P.; Awala, H.; Ghoy, J.-P.; Vicente, A.; Ling, T.C.; Ng, Y.H.; Mintova, S.; Adam, F. Effects of ultrasonic irradiation on crystallization and structural properties of EMT-type zeolite nanocrystals. *Mater. Chem. Phys.* **2015**, *159*, 38–45. [[CrossRef](#)]
16. Derakhshankhah, H.; Hajipour, M.J.; Barzegari, E.; Lotfabadi, A.; Ferdousi, M.; Saboury, A.A.; Ng, E.P.; Raoufi, M.; Awala, H.; Mintova, S. Zeolite nanoparticles inhibit A β -fibrinogen interaction and formation of a consequent abnormal structural clot. *ACS Appl. Mater. Interfaces* **2016**, *8*, 30768–30779. [[CrossRef](#)]
17. Choo, M.-Y.; Oi, L.E.; Ling, T.C.; Ng, E.-P.; Lin, Y.-C.; Centi, G.; Juan, J.C. Deoxygenation of Triolein to green diesel in the H₂-free condition: Effect of transition metal oxide supported on Zeolite Y. *J. Anal. Appl. Pyrolysis* **2020**, *147*, 104797. [[CrossRef](#)]

18. Wang, D.; Jangjou, Y.; Liu, Y.; Sharma, M.K.; Luo, J.; Li, J.; Kamasamudram, K.; Epling, W.S. A comparison of hydrothermal aging effects on NH₃-SCR of NO_x over Cu-SSZ-13 and Cu-SAPO-34 catalysts. *Appl. Catal. B Environ.* **2015**, *165*, 438–445. [[CrossRef](#)]
19. Leistner, K.; Mihai, O.; Wijayanti, K.; Kumar, A.; Kamasamudram, K.; Currier, N.W.; Yezerets, A.; Olsson, L. Comparison of Cu/BEA, Cu/SSZ-13 and Cu/SAPO-34 for ammonia-SCR reactions. *Catal. Today* **2015**, *258*, 49–55. [[CrossRef](#)]
20. Tian, P.; Wei, Y.; Ye, M.; Liu, Z. Methanol to olefins (MTO): From fundamentals to commercialization. *ACS Catal.* **2015**, *5*, 1922–1938. [[CrossRef](#)]
21. Wang, X.; Liu, Z.; Wei, X.; Guo, F.; Li, P.; Guo, S. Synthesis of 2, 6-dimethylnaphthalene over SAPO-11, SAPO-5 and mordenite molecular sieves. *Braz. J. Chem. Eng.* **2017**, *34*, 295–306. [[CrossRef](#)]
22. Wei, X.-L.; Lu, X.-H.; Zhang, T.-J.; Chu, X.; Zhou, D.; Nie, R.-F.; Xia, Q.-H. Synthesis and catalytic application of SAPO-5 by dry-gel conversion for the epoxidation of styrene with air. *Microporous Mesoporous Mater.* **2015**, *214*, 80–87. [[CrossRef](#)]
23. Ahoba-Sam, C.; Erichsen, M.W.; Olsbye, U. Ethene and butene oligomerization over isostructural H-SAPO-5 and H-SSZ-24: Kinetics and mechanism. *Chin. J. Catal.* **2019**, *40*, 1766–1777. [[CrossRef](#)]
24. Li, G.; Wang, B.; Chen, B.; Resasco, D.E. Role of water in cyclopentanone self-condensation reaction catalyzed by MCM-41 functionalized with sulfonic acid groups. *J. Catal.* **2019**, *377*, 245–254. [[CrossRef](#)]
25. Grand, J.; Talapaneni, S.N.; Vicente, A.; Fernandez, C.; Dib, E.; Aleksandrov, H.A.; Vayssilov, G.N.; Retoux, R.; Boullay, P.; Gilson, J.-P. One-pot synthesis of silanol-free nanosized MFI zeolite. *Nat. Mater.* **2017**, *16*, 1010. [[CrossRef](#)]
26. Wang, W.; Zhang, W.; Chen, Y.; Wen, X.; Li, H.; Yuan, D.; Guo, Q.; Ren, S.; Pang, X.; Shen, B. Mild-acid-assisted thermal or hydrothermal dealumination of zeolite beta, its regulation to Al distribution and catalytic cracking performance to hydrocarbons. *J. Catal.* **2018**, *362*, 94–105. [[CrossRef](#)]
27. Sun, X.; Wang, J.; Chen, J.; Zheng, J.; Shao, H.; Huang, C. Dehydration of fructose to 5-hydroxymethylfurfural over MeSAPOs synthesized from bauxite. *Microporous Mesoporous Mater.* **2018**, *259*, 238–243. [[CrossRef](#)]
28. Ketzer, F.; Celante, D.; de Castilhos, F. Catalytic performance and ultrasonic-assisted impregnation effects on WO₃/USY zeolites in esterification of oleic acid with methyl acetate. *Microporous Mesoporous Mater.* **2020**, *291*, 109704. [[CrossRef](#)]
29. Kim, K.; Ryoo, R.; Jang, H.-D.; Choi, M. Spatial distribution, strength, and dealumination behavior of acid sites in nanocrystalline MFI zeolites and their catalytic consequences. *J. Catal.* **2012**, *288*, 115–123. [[CrossRef](#)]
30. Freitas, E.F.; Araujo, A.A.; Paiva, M.F.; Dias, S.C.; Dias, J.A. Comparative acidity of BEA and Y zeolite composites with 12-tungstophosphoric and 12-tungstosilicic acids. *Mol. Catal.* **2018**, *458*, 152–160. [[CrossRef](#)]
31. Chen, L.; Ping, Z.; Chuah, G.; Jaenicke, S.; Simon, G. A comparison of post-synthesis alumination and sol-gel synthesis of MCM-41 with high framework aluminum content. *Microporous Mesoporous Mater.* **1999**, *27*, 231–242. [[CrossRef](#)]
32. Choudhary, V.R.; Jana, S.K. Benzylolation of benzene and substituted benzenes by benzyl chloride over InCl₃, GaCl₃, FeCl₃ and ZnCl₂ supported on clays and Si-MCM-41. *J. Mol. Catal. A Chem.* **2002**, *180*, 267–276. [[CrossRef](#)]
33. Hu, X.; Chuah, G.K.; Jaenicke, S. Room temperature synthesis of diphenylmethane over MCM-41 supported AlCl₃ and other Lewis acids. *Appl. Catal. A Gen.* **2001**, *217*, 1–9. [[CrossRef](#)]
34. Lili, Q.; Min, J.; Xinkui, W.; Min, H.; Tianxi, C. Isomerization of bridged tetrahydrodicyclopentadiene over AlCl₃/MCM-41 catalyst. *Chin. J. Catal.* **2010**, *31*, 383–385.
35. Sadjadi, S.; Lazzara, G.; Heravi, M.M.; Cavallaro, G. Pd supported on magnetic carbon coated halloysite as hydrogenation catalyst: Study of the contribution of carbon layer and magnetization to the catalytic activity. *Appl. Clay Sci.* **2019**, *182*, 105299. [[CrossRef](#)]
36. Sadjadi, S.; Lazzara, G.; Malmir, M.; Heravi, M.M. Pd nanoparticles immobilized on the poly-dopamine decorated halloysite nanotubes hybridized with N-doped porous carbon monolayer: A versatile catalyst for promoting Pd catalyzed reactions. *J. Catal.* **2018**, *366*, 245–257. [[CrossRef](#)]
37. Clark, J.H. Green chemistry: Challenges and opportunities. *Green Chem.* **1999**, *1*, 1–8. [[CrossRef](#)]
38. Choo, M.-Y.; Juan, J.C.; Oi, L.E.; Ling, T.C.; Ng, E.-P.; Noorsaadah, A.R.; Centi, G.; Lee, K.T. The role of nanosized zeolite Y in the H₂-free catalytic deoxygenation of triolein. *Catal. Sci. Technol.* **2019**, *9*, 772–782. [[CrossRef](#)]

39. Choudhary, V.R.; Mantri, K.; Jana, S.K. Highly selective Si-MCM-41 supported InCl_3 , GaCl_3 , FeCl_3 and ZnCl_2 catalysts for low temperature esterification of tert-butanol by acetic anhydride. *Microporous Mesoporous Mater.* **2001**, *47*, 179–183. [CrossRef]
40. International Zeolite Association. Database of Zeolite Structures. 2020. Available online: <http://www.iza-structure.org/databases/> (accessed on 20 April 2020).
41. Adam, F.; Appaturi, J.N.; Ng, E.-P. Halide aided synergistic ring opening mechanism of epoxides and their cycloaddition to CO_2 using MCM-41-imidazolium bromide catalyst. *J. Mol. Catal. A Chem.* **2014**, *386*, 42–48. [CrossRef]
42. Khoo, D.Y.; Awala, H.; Mintova, S.; Ng, E.-P. Synthesis of AlPO-5 with diol-substituted imidazolium-based organic template. *Microporous Mesoporous Mater.* **2014**, *194*, 200–207. [CrossRef]
43. Geng, L.; Dong, H.; Liu, X.; Zhang, B. Efficient manipulation of continuous AFI-type aluminophosphate membranes with distinctive microstructures on macroporous $\alpha\text{-Al}_2\text{O}_3$ substrates. *Molecules* **2018**, *23*, 1127. [CrossRef] [PubMed]
44. Chen, J.; Wright, P.; Natarajan, S.; Thomas, J. Understanding the Brønsted acidity of SAPO-5, SAPO-17, SAPO-18 and SAPO-34 and their catalytic performance for methanol conversion to hydrocarbons. In *Studies in Surface Science and Catalysis*; Elsevier: Amsterdam, The Netherlands, 1994; Volume 84, pp. 1731–1738.
45. Pfnennig, B.W. *Principles of Inorganic Chemistry*; John Wiley & Sons: Hoboken, NJ, USA, 2015.
46. Zerk, T.J.; Bernhardt, P.V. Redox-Coupled structural changes in copper chemistry: Implications for atom transfer catalysis. *Coord. Chem. Rev.* **2018**, *375*, 173–190. [CrossRef]
47. Ginés-Molina, M.J.; Ahmad, N.H.; Mérida-Morales, S.; García-Sancho, C.; Mintova, S.; Eng-Poh, N.; Maireles-Torres, P. Selective conversion of glucose to 5-Hydroxymethylfurfural by using L-type zeolites with different morphologies. *Catalysts* **2019**, *9*, 1073. [CrossRef]
48. Kumar, N.; Villegas, J.I.; Salmi, T.; Murzin, D.Y.; Heikkilä, T. Isomerization of n-butane to isobutane over Pt-SAPO-5, SAPO-5, Pt-H-mordenite and H-mordenite catalysts. *Catal. Today* **2005**, *100*, 355–361. [CrossRef]
49. Obermayer, D.; Znidar, D.; Glotz, G.; Stadler, A.; Dallinger, D.; Kappe, C.O. Design and performance validation of a conductively heated sealed-vessel reactor for organic synthesis. *J. Org. Chem.* **2016**, *81*, 11788–11801. [CrossRef]
50. Ahmad, N.H.; Daou, T.J.; Maireles-Torres, P.; Zaarour, M.; Mintova, S.; Ling, T.-C.; Ng, E.-P. Morphological effects on catalytic performance of LTL zeolites in acylation of 2-methylfuran enhanced by non-microwave instant heating. *Mater. Chem. Phys.* **2020**, *244*, 122688. [CrossRef]
51. Ji, Y.; Pan, J.; Dauenhauer, P.; Gorte, R.J. Probing direct carbon-carbon acylation of furans and long-chain acids over H-ZSM-5. *Appl. Catal. A Gen.* **2019**, *577*, 107–112. [CrossRef]
52. Wang, Z.; Li, H.; Zhao, W.; Yang, S. Low-Temperature and solvent-free production of biomass-derived diesel-range C17 precursor via one-pot cascade acylation-alkylation over Sn^{4+} -montmorillonite. *J. Ind. Eng. Chem.* **2018**, *66*, 325–332. [CrossRef]
53. Xiong, Y.; Chen, W.; Zeng, A. Optimization for catalytic performances of H β zeolite in the acylation of 2-methylfuran by surface modification and solvents effect. *Res. Chem. Intermed.* **2017**, *43*, 1557–1574. [CrossRef]
54. Koehle, M.; Zhang, Z.; Goulas, K.A.; Caratzoulas, S.; Vlachos, D.G.; Lobo, R.F. Acylation of methylfuran with Brønsted and Lewis acid zeolites. *Appl. Catal. A Gen.* **2018**, *564*, 90–101. [CrossRef]
55. Ghrear, T.M.A.; Wong, K.L.; Tan, S.H.; Ling, T.C.; Awala, H.; Ng, E.-P. Organotemplate-Free Cs-ABW nanozeolite as highly reactive and recyclable catalyst for Henry reaction between benzaldehyde and nitroethane. *Turk. J. Chem.* **2019**, *43*, 568–581. [CrossRef]
56. Rothenberg, G. *Catalysis: Concepts and Green Applications*; John Wiley & Sons: Hoboken, NJ, USA, 2017.
57. Liu, F.; Wang, T.; Zheng, Y.; Wang, J. Synergistic effect of Brønsted and Lewis acid sites for the synthesis of polyoxymethylene dimethyl ethers over highly efficient $\text{SO}_4^{2-}/\text{TiO}_2$ catalysts. *J. Catal.* **2017**, *355*, 17–25. [CrossRef]

